

Volumetric Displacement Effects of Dispersed Phase on the Euler-Lagrange Prediction of a Dense Spray

Pedram Pakseresht^a, Sourabh V. Apte^{a,*}

^a*School of Mechanical, Industrial and Manufacturing Engineering, Oregon State University, Corvallis, OR 97331, USA*

Abstract

Accurate prediction of a dense spray using an Euler-Lagrange approach is challenging because of high volume fraction of the dispersed phase due to subgrid cluster of droplets. To accurately model dense sprays, one needs to capture this effect by taking into account the spatio-temporal changes in the volume fraction of the carrier phase due to the motion and presence of the dispersed phase. This leads to zero-Mach number, variable density equations which are commonly neglected in the standard two-way coupling spray simulations. Using pressure-based solvers, this gives rise to a source term in the pressure Poisson equation and a non-divergence free velocity field. To validate the predictive capability of such approach, an atomized non-evaporating dilute particulate round jet is first examined using Large Eddy Simulation coupled with Point-Particle approach and then higher volume loadings up to 38% are investigated with and without taking into account the volumetric displacement effects. It is shown that for volume loadings above 5%, the volumetric displacement effects enhance dynamics of the flow resulting in a higher stream-wise mean and r.m.s. velocities compared to the results of standard two-way coupling. This is more pronounced for the near field of the jet where local volume fraction of the dispersed phase is relatively high. This enhancement is conjectured to be due to the velocity divergence effect due to the modified continuity equation where spatio-temporal variations in volume fraction of the carrier phase increases velocity in the regions of high void fraction.

1. Introduction

Liquid spray atomization plays an important role in analyzing the combustion process in many propulsion related applications. Disintegration of injecting liquid fuel which occurs

*Corresponding author. 204 Rogers Hall, Corvallis, OR 97331, USA. Tel: +1 541 737 7335, Fax: +1 541 737 2600.

Email addresses: pakserrep@oregonstate.edu (Pedram Pakseresht),
Sourabh.Apte@oregonstate.edu (Sourabh V. Apte)

Preprint submitted to ICLASS 2018

in two steps; primary atomization followed by secondary atomization makes this process a complex flow. This has opened a new field of study for investigating and modeling this flow. In the traditional approaches for spray modeling, the dynamics of the liquid/air interface are not resolved. Instead, the liquid phase is modeled through either an Eulerian approach in which droplets are considered to be as a continuous liquid phase or Lagrangian Point-Particle/Parcel (PP) method where droplets are assumed subgrid and their motion is captured by force closures such as drag, buoyancy, pressure, etc., while the effect of the droplets on the gas phase is modeled through two-way coupling of mass, momentum, and energy exchange Dukowicz (1980). In such scenario, volume fraction of droplets compared to the computational cell must be very small so that the Point-Particle approach could be practical and feasible. This restriction, however, prevents Euler-Lagrange approaches from applying to regions with high void fractions such as near the nozzle exit where primary atomization takes place. This led researchers to perform Eulerian-Lagrangian Spray Atomization (ELSA) approach which couples the Eulerian mixing description for primary atomization (LES/DNS) with Lagrangian formulation (PP method) for secondary breakup Blokkeel et al. (2003); Lebas et al. (2005). These models were originally derived in the context of RANS turbulence models and assume infinite Weber number, however, extensions to LES formulations have been recently proposed by Chesnel et al. (2011b,a). Recently, hybrid approaches of DNS method for the primary atomization region along with LES coupled with Lagrangian Point-Particle/Parcel approach for solving the gas and liquid phases respectively in the secondary atomization region have been developed by, e.g., Herrmann (2010, 2011) among others. These hybrid approaches have shown quite success in predicting atomization even in complex aircraft engine injectors, yet on the one hand they are still computationally expensive. On the other hand, for the secondary atomization, the spatio-temporal variations in volume fraction of the carrier phase is still neglected in Euler-Lagrange approaches. This effect can be significant particularly in atomizing sprays where volume fraction of the injecting liquid phase is in the order of one near the nozzle exit. Therefore, ignoring this effect would eliminate the real dynamics of such flows in which the liquid phase displaces a remarkable portion of the gaseous phase.

Therefore, in this work, to take advantage of computationally less expensive Euler-Lagrange approaches as well as for more accurate predictions of dense spray flows, an Euler-Lagrange approach modified with spatio-temporal variations in the carrier phase volume fraction is applied Anderson and Jackson (1967); Dukowicz (1980); Joseph et al. (1990). In order to distinguish this method from the standard Euler-Lagrange two-way coupling approaches, we refer to this model as volumetric coupling in line with work of Cihonski et al. (2013). Although there have been some studies showing the insignificance of volumetric coupling compared to the standard two-way coupling for dilute regimes (e.g., Vreman et al. (2004)), several works have depicted the importance of this unique coupling. Apte et al. (2008) illustrated a large difference in prediction of particle dispersion in fluidization process using this approach compared to the standard Euler-Lagrange approach. Ferrante and Elghobashi (2004) observed that taking into account the volumetric displacement effect results in accurately capturing drag reduction in the boundary layer over a flat plate. In line with previous works, Cihonski et al. (2013) showed that even under dilute

loading (small number of bubbles entrained in a vortex ring), accounting for this effect can significantly alter the vortex core for certain combinations of the vortex strengths and bubble sizes. In the current work, similar formulation is applied to an atomized non-evaporating particulate jet flow to only focus on the volumetric displacement effect rather than atomization processes. We start looking a dilute particulate round jet as a validation case and then increasing the corresponding volume loading of the dispersed phase (here solid particles) up to 38% while keeping other flow parameters constant. Four different volume loadings are studied here to investigate the importance of volumetric displacement effect at different loadings explained in the next sections.

2. Methodology

An Euler–Lagrange approach is used to simulate the particle-turbulence interactions involved in dense spray flows. Fluid motion is captured through solving the Navier-Stokes as well as continuity equations in an Eulerian framework using large eddy simulation (LES) while motion of particles is modeled in a Lagrangian framework using available force closures, the so-called Point-Particle approach Maxey (1987); Elghobashi (1991); Squires and Eaton (1991). Governing equations on these two phases are explained in the following sections in detail.

2.1. Dispersed Phase Formulation

Small particles (i.e., smaller than the resolved fluid length scale) are tracked through the Newton second law of motion given the forces exerted by fluid as shown in Equation 1 Maxey and Riley (1983). Unlike body-fitted approaches (e.g. Pakseresht et al. (2012)), the no-slip condition on the surface of particles is not imposed in this approach. According to this, one can obtain velocity components, \mathbf{u}_p , as well as position, \mathbf{x}_p , of each individual particle of mass m_p .

$$\begin{aligned} \frac{d}{dt}(\mathbf{x}_p) &= \mathbf{u}_p \\ \frac{d}{dt}(\mathbf{u}_p) &= \frac{1}{m_p} (\mathbf{F}_g + \mathbf{F}_{pr} + \mathbf{F}_d + \mathbf{F}_{l,Saff} + \mathbf{F}_{l,Mag} + \mathbf{F}_{am}) \end{aligned} \tag{1}$$

Equation 1 shows all possible forces including gravitational body force, \mathbf{F}_g , hydrostatic pressure gradient, \mathbf{F}_{pr} , shear induced lift force Saffman (1965), $\mathbf{F}_{l,Saff}$, Magnus effect due to particle rotation Rubinow and Keller (1961), \mathbf{F}_{Mag} , as well as added mass Auton (1983), \mathbf{F}_{am} . In order to capture more accurately particle-turbulence interactions in a dense spray regime, the drag closure by Tenneti et al. (2011), \mathbf{F}_d , is employed here where coefficient of drag, $C_d(Re_p, \theta_p)$ accounts for local volume fraction of dispersed phase as well as finite particle Reynolds number. It has been observed that the Basset history force does not remarkably affect motion of particles in the presence of steady drag force Maxey and Riley (1983); Bagchi and Balachandar (2003), therefore, this force is excluded in this study. All aforementioned forces above are given in Equations 2-7 as follow;

$$\mathbf{F}_g = (\rho_p - \rho_g)V_p\mathbf{g} \quad ; \quad g = -9.81m/s^2 \quad (2)$$

$$\mathbf{F}_{pr} = -V_p\nabla P|_p \quad (3)$$

$$\mathbf{F}_{l,Saff} = m_p C_l \frac{\rho_f}{\rho_p} (\mathbf{u}_{f|p} - \mathbf{u}_p) \times (\nabla \times \mathbf{u}_f)|_p, \quad \text{and} \quad C_l = \frac{1.61 \times 6}{\pi d_p} \sqrt{\frac{\mu_f}{\rho_f} |(\nabla \times \mathbf{u}_f)|_p} \quad (4)$$

$$\mathbf{F}_{l,Mag} = C_{mag} \frac{\mathbf{u}_{rel} \times \boldsymbol{\Omega}_{rel}}{|\boldsymbol{\Omega}_{rel}|} \left(\frac{1}{2} \rho_f |\mathbf{u}_{rel}| A \right), \quad \text{and} \quad C_{mag} = \min(0.5, 0.25 \frac{d_p |\omega_{rel}|}{|u_{rel}|}) \quad (5)$$

$$\mathbf{F}_{am} = m_p C_{am} \frac{\rho_f}{\rho_p} \left(\frac{D\mathbf{u}_{f|p}}{Dt} - \frac{d\mathbf{u}_p}{dt} \right), \quad C_{am} = 0.5 \quad (6)$$

$$\begin{aligned} \mathbf{F}_d &= m_p \frac{C_d(Re_p, \theta_p)}{\tau_p} (\mathbf{u}_{f|p} - \mathbf{u}_p) \\ C_d(Re_p, \theta_p) &= (1 - \theta_p) \left(\frac{C_d(Re_p, 0)}{(1 - \theta_p)^3} + A + B \right), \\ A &= \frac{5.81\theta_p}{(1 - \theta_p)^3} + 0.48 \frac{\theta^{1/3}}{(1 - \theta_p)^4}, \\ B &= \theta_p^3 Re_p (0.95 + \frac{0.61\theta_p^3}{(1 - \theta_p)^2}), \\ C_d(Re_p, 0) &= 1 + 0.15 Re_p^{0.687}. \end{aligned} \quad (7)$$

where volume and volume fraction of each particle are represented by V_p and θ_p respectively. $\mathbf{u}_{rel} = \mathbf{u}_{f|p} - \mathbf{u}_p$ is the relative velocity between fluid (seen by particle) ($\mathbf{u}_{f|p}$) and particle (\mathbf{u}_p). On the other hand, $\tau_p = (\rho_p d_p^2)/(18\rho_f\mu_f\theta_p)$ and $Re_p = (\theta_{f|p}\rho_f|u_{rel}|d_p)/(\mu_f)$ are the respective particle relaxation time and particle Reynolds number modified by local volume fraction of the dispersed phase Finn et al. (2016).

2.2. Fluid Phase Formulation

Large eddy simulation (LES) is employed to solve the carrier phase equations in a structured Cartesian grid using finite volume discretization. A pressure based second order fractional time step method based on work of Finn et al. (2011) and Cihonski et al. (2013), adjusted to a co-located structured grid by Finn et al. (2016) is utilized here. To consider the effect of volume of carrier phase displaced by the motion and presence of particles, the volume filtered Navier-Stokes equations given in (8)-(9) are applied here Anderson and Jackson (1967); Joseph et al. (1990). Despite typical incompressible flows, the spatio-temporal variations in particle volume fraction generate a non-divergence free velocity field in the flow.

$$\frac{\partial(\rho_f\theta_f)}{\partial t} + \nabla \cdot (\rho_f\theta_f\mathbf{u}_f) = 0. \quad (8)$$

$$\frac{\partial(\rho_f\theta_f\mathbf{u}_f)}{\partial t} + \nabla \cdot (\rho_f\theta_f\mathbf{u}_f\mathbf{u}_f) = -\theta_f\nabla P + \nabla \cdot [\mu_f\theta_f(\nabla\mathbf{u}_f + \nabla\mathbf{u}_f^T)] + \theta_f\rho_f\mathbf{g} + \mathbf{F}_{p\rightarrow f}. \quad (9)$$

where ρ_f , θ_f , and \mathbf{u}_f are density, volume fraction, and velocity of the carrier phase respectively. Volume fraction of carrier phase is calculated as $\theta_f = 1 - \theta_p$, where θ_p corresponds to volume fraction of particles located in each computational cell. The point-particle forces, $\mathbf{F}_{p\rightarrow f}$, include the equal and opposite reaction forces from the particle surface forces except the pressure force. Accordingly, it is crucial to define a function to project Lagrangian quantities of dispersed phase back to the continuous field as well as interpolate carrier phase properties to the particles' position. Gaussian function Apte et al. (2008) for both interpolation and projection purposes is employed with a dynamic bandwidth equal to the local grid size of each particle's neighbourhood. It is worth mentioning that given $\theta_f = 1$, the above formulation switches to the standard two-way coupling where volumetric displacement effects of the carrier phase is then neglected. For large-eddy simulation, the equations above should be spatially filtered using density weighted Favre averaging Hutter and Jöhnk (2004). For turbulent flows, the Favre averaged equations then have the same form as Equation 9 with the exception that the left-hand side of the momentum equation consists of an unclosed subgrid stress term,

$$\tau_{ij} = \overline{\rho_f\theta_f u_i u_j} - \overline{\rho_f\theta_f u_i} \overline{\rho_f\theta_f u_j} / \overline{\rho_f\theta_f} \quad (10)$$

denoting $\rho = \rho_f\theta_f$, Favre-averaged velocity field can be obtained as $\overline{\rho\tilde{u}_i} = \overline{\rho u_i}$. The unclosed subgrid-scale stresses can be closed by use of a Smagorinsky model with a dynamic procedure for the calculation of the model coefficient and eddy viscosity Germano et al. (1991); Moin et al. (1991).

$$\mu_T = -C_S \overline{\rho_f\theta_f} \Delta^2 S(\tilde{u}) \quad ; \quad \Delta = V_{cv}^{1/3} \quad ; \quad S(\tilde{u}) = \left(\frac{1}{2} S_{ij} S_{ij}\right)^{1/2} \quad (11)$$

where V_{cv} is the volume of a grid cell, and the model constant C_S is obtained using the dynamic procedure and a test filter of twice the size of the control volume. The governing equation then is obtained in terms of the filtered velocity fields \tilde{u} and the fluid viscosity μ_f us changed to $\mu_{eff} = \mu_f + \mu_T$ accounting for the eddy viscosity.

3. Numerical Results

The numerical scheme explained above has been widely applied to and validated for different applications (Shams et al., 2011; Cihonski et al., 2013; Pakseresht et al., 2014, 2015, 2016; Finn et al., 2016; Pakseresht et al., 2017; Pakseresht and Apte, 2017, 2018; He et al., 2018). Besides, in this work the accuracy and robustness of the method is also enforced on an atomized non-evaporating turbulent round jet laden with dilute regime of inertial

Case	$d_p(\mu m)$	Re_j	S.G.	$[\overline{\theta_p}]_{inlet}$	$N_p(million)$	Inter-particle collision	Coupling type
A	105	5712	2122.24	0.00047	0.15	No	2-way w/wo volumetric effect
B	105	5712	2122.24	0.047	0.34	Yes	2-way w/wo volumetric effect
C	105	5712	2122.24	0.188	1.3	Yes	2-way w/wo volumetric effect
D	105	5712	2122.24	0.376	2.56	Yes	2-way w/wo volumetric effect
E	105	5712	2122.24	0.188	1.3	Yes	1-way w/wo volumetric effect

Table 1: Particle and flow properties for different cases.

particles. Then, to investigate the volumetric displacement effects of dispersed phase, four denser cases, i.e., B-E shown in Table 1 are performed. In these cases all parameters except volume loading are the same as those in case A. Case E is similar to case D yet instead of two-way coupling, the momentum force exchange term is excluded. As listed in Table 1, for cases B-D, the volumetric coupling is compared to the corresponding standard two-way coupling while for case E one-way coupling is compared to its modification by volumetric displacement effects (volumetric formulation). An experimental data Mostafa et al. (1989) is only available for case A while no data is available for higher loadings. This case validates our numerical results. For further results on the validation see Pakseresht and Apte (2019a). For other cases, only numerical results from different couplings are compared together to investigate the volumetric displacement effects. In all studied cases here, a Cartesian structured grid is used for solving the flow in a rectangular computational domain with size of $6d_{jet} \times 6d_{jet} \times 14d_{jet}$ in cross-sectional and longitudinal directions, respectively. Inflow data over several flow through times is generated a priori and read at each flow time step to specify the fluid velocity components at the inlet. Convective outflow boundary condition is applied at the outlet while slip boundary condition is enforced for other sides of the computational domain. As given in table 1, particles of 105 micron with specific gravity, $S.G. = \rho_p/\rho_f$, of 2122.24 are injected at the nozzle exit based on different volume loadings. Reynolds number of clear jet denoted by $Re_j = \rho_f U_j d_j / \mu_f = 5712$ is defined based on the jet bulk velocity, $U_j = 3.546m/s$, jet nozzle diameter, $d_j = 0.0253m$, and the carrier phase properties for air, $\rho_f = 1.178kg/m^3$ and $\mu_f = 1.8502 \times 10^{-5}kg/(m.s)$ corresponding to the experimental work of Mostafa et al. (1989).

Regarding dispersed phase, measured data at $x/d_{jet} = 0.04$ in the corresponding experiment of case A is used to prescribe mean and r.m.s. velocities in all simulations for injecting particles in the already statistically stable turbulent jet flow. Numerical results at each nozzle distance are obtained based on the azimuthal averaging in space as well as long enough time averaging. Total number of injecting particles for each case required at each time step (Δt_f) can be calculated based on the given volume loading, particle's diameter and jet bulk velocity as $n_p = 6[\overline{\theta_p}]_{inlet} d_j^2 U_j \Delta t_f / 4d_p^3$. Figures 1 and 2 show the comparison of our numerical simulation with experimental data for both carrier and dispersed phases of case A respectively. All results are plotted in normalized radial direction based on jet radius of r_j . Mean velocities of the carrier and dispersed phases are normalized with bulk velocity of the clear jet, U_j , and local centreline velocity of the laden jet at each nozzle distance, U_c , respectively. A good agreement between numerical results and corresponding experiment on mean velocity of two phases is achieved. On each plot, volumetric coupling prediction

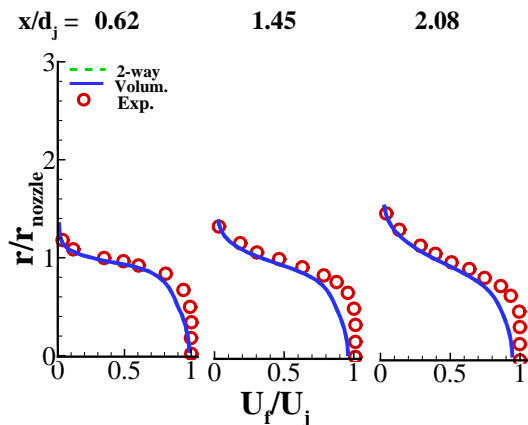


Figure 1: Normalized mean velocity of the carrier phase based on two different couplings compared with experimental data of Mostafa et al. (1989)

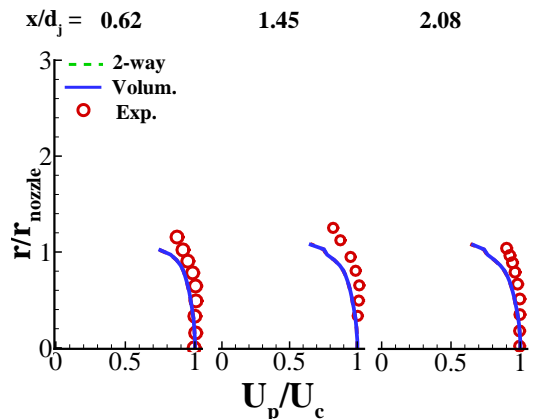


Figure 2: Normalized mean velocity of the dispersed phase based on two different couplings compared with experimental data of Mostafa et al. (1989)

matches the results of standard two-way coupling. That would be expected as loading of the dispersed phase in case A is so dilute that even inter-particle collision is negligible and thus the dominant mechanism is only the two-way coupling Elgobashi (2006). This was also observed by Vreman et al. (2004) where they found insignificant difference between two-way and volumetric couplings for a channel flow laden with average solid volume fraction of $\overline{\theta_p} = 0.013$ (i.e., 1.3%).

3.1. Volumetric Displacement Effects

The purpose of this section is to study the volumetric displacement effects of dispersed phase onto the characteristics of the carrier phase compared with the predictions of common two-way Euler-Lagrange approaches where this effect is neglected. As the regime in cases B-E is dense, therefore inter-particle collision is also required to account for. Soft-sphere model of Cundall and Strack (1979) is employed here. Collision parameters and formulation can be found in our earlier works, e.g., Finn et al. (2016); Pakseresht et al. (2017). A comparison between prediction of volumetric and standard two-way couplings on the mean and r.m.s. velocities of the carrier phase corresponding to cases B to D is performed here. Figures 3-5 depict the LES-PP results of cases B-D respectively for mean and r.m.s. velocities of the carrier phase. For case B as shown in Figure 3, slight difference exists between these two approaches with the maximum of 3% and 16% increase in the mean and r.m.s. velocities predicted by the volumetric coupling right at the nozzle exit. However, this difference becomes more pronounced and distinguishable with increasing particles' loading such as those in cases C and D plotted in Figures 4 and 5 respectively. As illustrated in these plots, volumetric coupling predicts higher mean and r.m.s. velocities remarkably compared to the standard two-way coupling. Furthermore, one can see that the difference between two-way and volumetric couplings decreases with nozzle distance in all cases which could be conjectured due to spread and entrainment of the particulate jet which in turn decreases

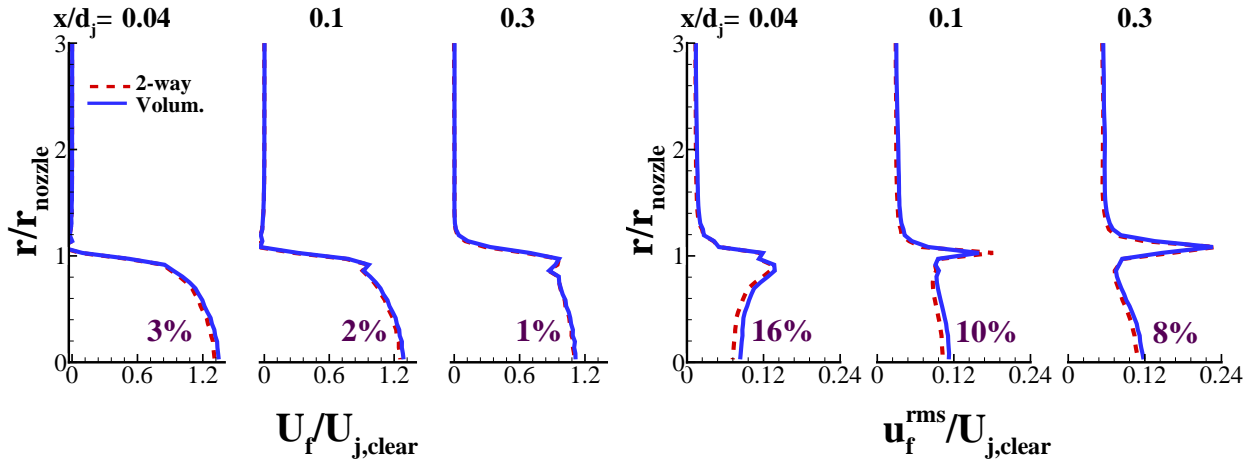


Figure 3: Normalized streamwise mean (left) and r.m.s. (right) velocities of the carrier phase for case B based on two different couplings.

the local volume fraction of the dispersed phase so does the difference between these two approaches farther away from the nozzle exit.

Better insight into the mechanisms of the particle-turbulence interactions involved in the volumetric coupling formulation can be further obtained by doing the force analysis. In the volumetric formulation, it is clear that the carrier phase sees the effects of particles not only through the force closures added to the momentum (standard two-way coupling) but also through the spatio-temporal variations in the carrier phase volume fraction due to presence of particles. It was shown in work of Cihonski et al. (2013) that this is the extra forces arise from volumetric formulation which differentiate this approach than standard two-way coupling. Figure 6 depicts a comparison between two-way and volumetric couplings predictions on the radial profile of particle feedback forces back onto the flow in the near field of the densest jet case (i.e., D). On the same plot, the most dominant force arises in the volumetric formulation observed by Cihonski et al. (2013), i.e., $\Delta V_6 = \rho_f \theta_f \mathbf{u}_f (\nabla \cdot \mathbf{u}_f)$ are also plotted. All forces on this plot are normalized by the jet momentum, i.e., $\rho_f A_j U_j^2$ in the stream-wise direction. It is clear that contribution of ΔV_6 is quite insignificant compared to the point-particle force both from volumetric coupling prediction. Furthermore, point particle force predicted by volumetric coupling formulation (i.e., $F_{p,vol}$) is almost twice than that of two-way coupling ($F_{p,2w}$). Likewise, fluid forces exerted onto the particles particularly right at the nozzle shown in Figure 7 reveal the fact that both drag as well as pressure forces are significantly larger in volumetric coupling prediction than those of standard two-way coupling. This shows that despite the work of Cihonski et al. (2013), here another mechanism must exist. This can be investigated by looking at the continuity equation used in volumetric coupling formulation where modified density may result in higher fluid velocity compared to the standard two-way coupling. To assess this, one can mask the effect of point-particle forces and purely investigate the volumetric displacement effects by looking at case E where a comparison between one-way coupling and its modification by volumetric

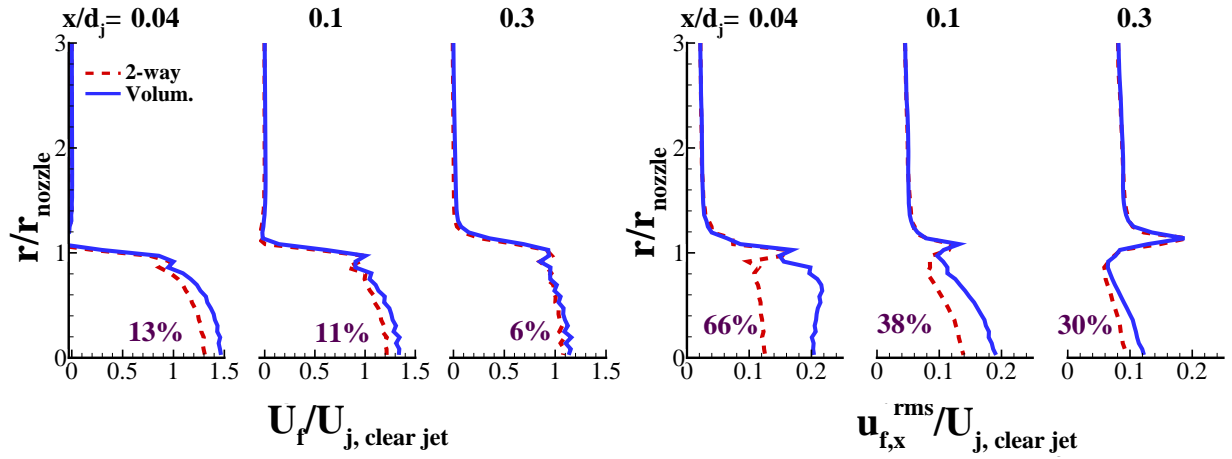


Figure 4: Normalized streamwise mean (left) and r.m.s. (right) velocities of the carrier phase for case C based on two different couplings.

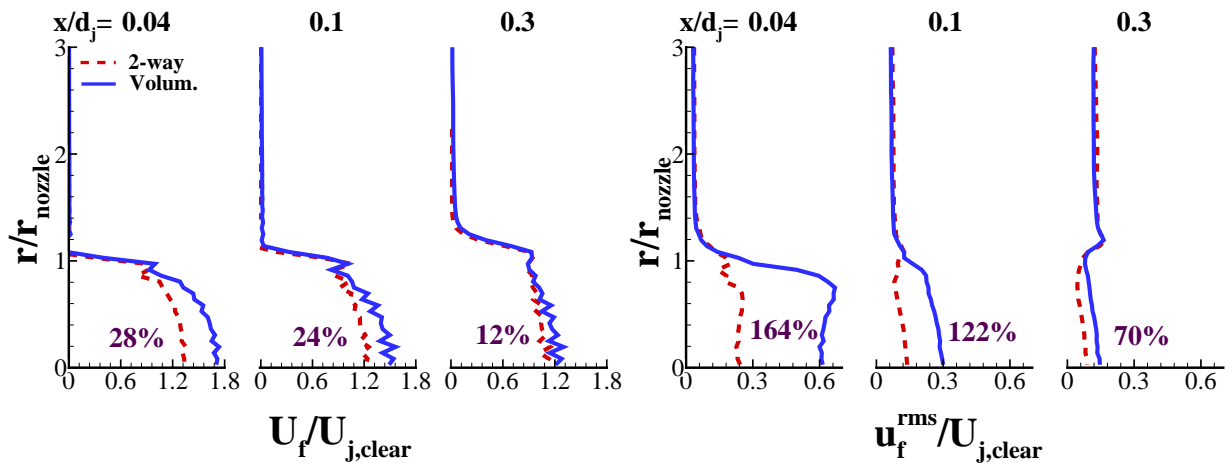


Figure 5: Normalized streamwise mean (left) and r.m.s. (right) velocities of the carrier phase for case D based on two different couplings.

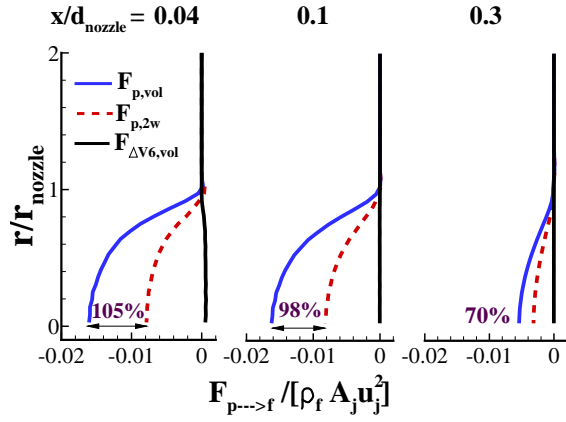


Figure 6: Contribution of particle reaction forces by two different coupling formulations normalized by the jet momentum.

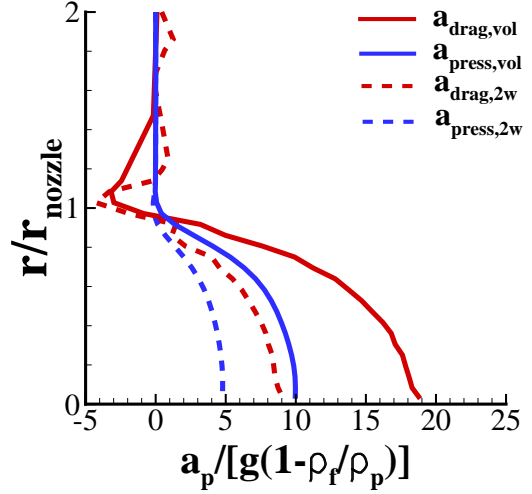


Figure 7: Contribution of exerted accelerations onto particles by two different coupling formulations normalized by Buoyancy.

formulation is performed and illustrated in Figure 8. Note that equations for standard one-way coupling can be simply obtained by recalling Equations 8 and 9 and giving $\theta_f = 1$ as well as $\mathbf{F}_{p \rightarrow f} = 0$. Likewise, modified one-way coupling is achieved by equaling $\mathbf{F}_{p \rightarrow f} = 0$ in the same equations, however, keeping spatio-temporal variations in the fluid volume fraction, i.e., $\theta_f \neq 1$. As depicted in Figure 8, a significant difference between these two couplings is observed for both mean and r.m.s. velocities at the nozzle exit. This can be again explained due to the fact that volumetric formulation solves carrier phase equations for less amount of volume (or density) due to presence of particles which in turn increases the corresponding velocity of the carrier phase. This observation is in line with work of Ferrante and Elghobashi (2004) where accurate prediction of the drag reduction in the boundary layer over a flat plate was shown to be due to the results of velocity divergence effect, i.e., accounting for spatio-temporal variations in fluid volume fraction. Further analyses particularly the influence of particle's Stokes number can be found in Pakseresht and Apte (2019b).

4. Summary and Conclusions

Accurate prediction of a dense spray flow using an Euler-Lagrange approach was presented. To accurately model this flow, volume of the carrier phase displaced by the motion and presence of dispersed phase was taken into account along with the standard two-way coupling point-particle forces employed in typical Euler-Lagrange approaches. To Investigate and quantify the volumetric displacement effects, various volume loadings ranging from dilute up to dense regime (38 %) were studied. It was observed that for volume loadings of equal and greater than 5% ($\overline{\theta}_p > 0.05$), volumetric coupling predicts higher mean velocity and turbulence intensities for the carrier phase in comparison with the standard two-way

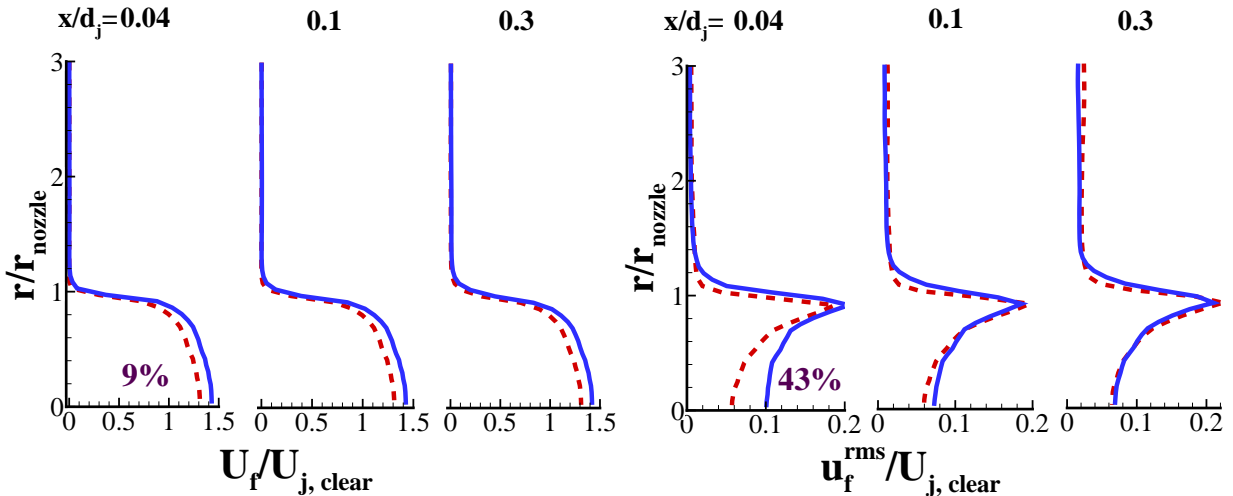


Figure 8: Normalized streamwise mean (left) and r.m.s. (right) velocities of the carrier phase for case C based on two different couplings.

coupling. In line with work of Ferrante and Elghobashi (2004), this enhancement was shown to be due to the velocity divergence effect as a result of modified continuity equation in which less amount of density in the region of high void fraction results in higher carrier phase velocity. Finally, the present formulation can be extended to further investigations of other fields such as energy harvesting (Kamrani Fard et al., 2019; Siala et al., 2020), among others, with the aid of micro particles.

5. Acknowledgements

The authors acknowledge the Texas Advanced Computing Center (TACC) at The University of Texas at Austin for providing HPC resources that have contributed to the research results reported within this paper. In addition, financial support from the National Aeronautics and Space Administration (NASA) is highly appreciated.

References

- Anderson, T. B., Jackson, R., 1967. Fluid mechanical description of fluidized beds. equations of motion. *Industrial & Engineering Chemistry Fundamentals* 6 (4), 527–539.
- Apte, S., Mahesh, K., Lundgren, T., 2008. Accounting for finite-size effects in simulations of disperse particle-laden flows. *International Journal of Multiphase Flow* 34 (3), 260–271.
- Auton, T. R., 1983. The dynamics of bubbles, drops and particles in motion in liquids. Ph.D. thesis, University of Cambridge.
- Bagchi, P., Balachandar, S., 2003. Effect of turbulence on the drag and lift of a particle. *Physics of fluids* 15 (11), 3496–3513.
- Blokkeel, G., Barbeau, B., Borghi, R., 2003. A 3d eulerian model to improve the primary breakup of atomizing jet. Tech. rep., SAE Technical Paper.
- Chesnel, J., Menard, T., Reveillon, J., Demoulin, F.-X., 2011a. Subgrid analysis of liquid jet atomization. *Atomization and Sprays* 21 (1).

- Chesnel, J., Reveillon, J., Menard, T., Demoulin, F.-X., 2011b. Large eddy simulation of liquid jet atomization. *Atomization and Sprays* 21 (9).
- Cihonski, A. J., Finn, J. R., Apte, S. V., 2013. Volume displacement effects during bubble entrainment in a travelling vortex ring. *Journal of Fluid Mechanics* 721, 225–267.
- Cundall, P., Strack, O., 1979. A discrete numerical model for granular assemblies. *Geotechnique* 29, 47–65.
- Dukowicz, J. K., 1980. A particle-fluid numerical model for liquid sprays. *Journal of Computational Physics* 35 (2), 229–253.
- Elghobashi, S., 1991. Particle-laden turbulent flows: direct simulation and closure models. *Applied Scientific Research* 48 (3-4), 301–314.
- Elghobashi, S., 2006. An updated classification map of particle-laden turbulent flows. In: *IUTAM Symposium on Computational Approaches to Multiphase Flow*. Springer, pp. 3–10.
- Ferrante, A., Elghobashi, S., 2004. On the physical mechanisms of drag reduction in a spatially developing turbulent boundary layer laden with microbubbles. *Journal of Fluid Mechanics* 503, 345–355.
- Finn, J., Shams, E., Apte, S. V., 2011. Modeling and simulation of multiple bubble entrainment and interactions with two dimensional vortical flows. *Physics of Fluids* 23 (2), 023301.
- Finn, J. R., Li, M., Apte, S. V., 2016. Particle based modelling and simulation of natural sand dynamics in the wave bottom boundary layer. *Journal of Fluid Mechanics* 796, 340–385.
- Germano, M., Piomelli, U., Moin, P., Cabot, W. H., 1991. A dynamic subgrid-scale eddy viscosity model. *Physics of Fluids A: Fluid Dynamics* 3 (7), 1760–1765.
- He, X., Karra, S., Pakseresht, P., Apte, S., Elghobashi, S., 2018. Effect of heated-air blanket on the dispersion of squames in an operating room. *International journal for numerical methods in biomedical engineering* 34 (5), e2960.
- Herrmann, M., 2010. A parallel eulerian interface tracking/lagrangian point particle multi-scale coupling procedure. *Journal of Computational Physics* 229 (3), 745–759.
- Herrmann, M., 2011. On simulating primary atomization using the refined level set grid method. *Atomization and Sprays* 21 (4).
- Hutter, K., Jöhnk, K., 2004. Continuum methods of physical modelling—continuum mechanics, dimensional analysis, turbulence.
- Joseph, D., Lundgren, T., Jackson, R., Saville, D., 1990. Ensemble averaged and mixture theory equations for incompressible fluid-particle suspensions. *International journal of multiphase flow* 16 (1), 35–42.
- Kamrani Fard, K., Ma, P., Prier, M., Liburdy, J., 2019. Numerical and experimental investigation of oscillating flexible foils with application in energy harvesting. *Bulletin of the American Physical Society* 64.
- Lebas, R., Blokkeel, G., Beau, P.-A., Demoulin, F.-X., 2005. Coupling vaporization model with the eulerian-lagrangian spray atomization (elsa) model in diesel engine conditions. Tech. rep., SAE Technical Paper.
- Maxey, M., 1987. The gravitational settling of aerosol particles in homogeneous turbulence and random flow fields. *Journal of Fluid Mechanics* 174, 441–465.
- Maxey, M. R., Riley, J. J., 1983. Equation of motion for a small rigid sphere in a nonuniform flow. *The Physics of Fluids* 26 (4), 883–889.
- Moin, P., Squires, K., Cabot, W., Lee, S., 1991. A dynamic subgrid-scale model for compressible turbulence and scalar transport. *Physics of Fluids A: Fluid Dynamics* 3 (11), 2746–2757.
- Mostafa, A., Mongia, H., McDonell, V., Samuelsen, G., 1989. Evolution of particle-laden jet flows—a theoretical and experimental study. *AIAA journal* 27 (2), 167–183.
- Pakseresht, P., Apte, S., 2018. Volumetric displacement effects of the gaseous phase on the euler-lagrange prediction of spray atomization. *Bulletin of the American Physical Society*.
- Pakseresht, P., Apte, S., Finn, J., 2014. Interactions of turbulence and sediment particles in an open channel flow. In: *APS Meeting Abstracts*.
- Pakseresht, P., Apte, S., Finn, J., 2015. Dns with discrete element modeling of suspended sediment particles in an open channel flow. In: *APS Division of Fluid Dynamics Meeting Abstracts*.
- Pakseresht, P., Apte, S., Finn, J., 2016. Dns-dem of suspended sediment particles in an open channel flow. In: *APS Meeting Abstracts*.

- Pakseresht, P., Apte, S. V., 2017. Prediction of a densely loaded particle-laden jet using a euler-lagrange dense spray model. In: APS Division of Fluid Dynamics Meeting Abstracts.
- Pakseresht, P., Apte, S. V., 2019a. Modeling the dense spray regime using an euler-lagrange approach with volumetric displacement effects. arXiv preprint arXiv:1910.00746.
- Pakseresht, P., Apte, S. V., 2019b. Volumetric displacement effects in euler-lagrange les of particle-laden jet flows. *International Journal of Multiphase Flow* 113, 16–32.
- Pakseresht, P., Apte, S. V., Finn, J. R., 2017. On the predictive capability of dns-dem applied to suspended sediment-turbulence interactions. In: ASME 2017 Fluids Engineering Division Summer Meeting. American Society of Mechanical Engineers Digital Collection.
- Pakseresht, P., Bahrainian, S. S., Bahoosh Kazerooni, R., 2012. An algorithm in element deletion process used in moving three zones unstructured grid for arbitrary relative motion of two objects. In: Proceedings of 3rd International Conference on Theoretical and Applied Mechanics, Athens, Gr.
- Rubinow, S., Keller, J. B., 1961. The transverse force on a spinning sphere moving in a viscous fluid. *Journal of Fluid Mechanics* 11 (03), 447–459.
- Saffman, P., 1965. The lift on a small sphere in a slow shear flow. *Journal of fluid mechanics* 22 (02), 385–400.
- Shams, E., Finn, J., Apte, S., 2011. A numerical scheme for euler-lagrange simulation of bubbly flows in complex systems. *International Journal for Numerical Methods in Fluids* 67 (12), 1865–1898.
- Siala, F. F., Kamrani Fard, K., Liburdy, J. A., 2020. Experimental study of inertia-based passive flexibility of a heaving and pitching airfoil operating in the energy harvesting regime. *Physics of Fluids* 32 (1), 017101.
- Squires, K. D., Eaton, J. K., 1991. Preferential concentration of particles by turbulence. *Physics of Fluids A: Fluid Dynamics* 3 (5), 1169–1178.
- Tenneti, S., Garg, R., Subramaniam, S., 2011. Drag law for monodisperse gas–solid systems using particle-resolved direct numerical simulation of flow past fixed assemblies of spheres. *International journal of multiphase flow* 37 (9), 1072–1092.
- Vreman, A., Geurts, B. J., Deen, N. G., Kuipers, J., 2004. Large-eddy simulation of a particle-laden turbulent channel flow. In: *Direct and large-eddy simulation V*. Springer, pp. 271–278.